Introduction of TiO_2 in CuI for its Improved Performance as a p-type Transparent Conductor

Vidur Raj[1,], Teng Lu[2], Mark Lockrey[3], Rong Liu[4], Felipe Kremer[5], Li Li[3], Yun Liu[2], Hark Hoe Tan[1,*], and Chennupati Jagadish[1]*

[1]Research School of Physics and Engineering, The Australian National University, Canberra, ACT 2601 Australia

[2]Research School of Chemistry, The Australian National University, Canberra ACT 2601, Australia

[3]Australian National Fabrication Facility, Research School of Physics and Engineering, The Australian National University, Canberra, ACT 2601, Australia

[4]Secondary Ion Mass Spectrometry Facility, Office of the Deputy Vice-Chancellor (R&D), Western Sydney University, Penrith, NSW 2751, Australia

[5]Centre for Advanced Microscopy, The Australian National University, Canberra, ACT 2601, Australia

KEYWORDS: copper iodide (CuI), transparent conductor, flexible electronics

ABSTRACT

The challenges of making high performance, low temperature processed, p-type transparent conductors (TCs) have been the main bottleneck for the development of flexible transparent

electronics. Though a few p-type transparent conducting oxides (TCOs) have shown promising results, they need high processing temperature to achieve the required conductivity which makes them unsuitable for organic and flexible electronic applications. Copper iodide is a wide band gap p-type semiconductor that can be heavily doped at low temperature (<100 ºC) to achieve conductivity comparable or higher than many of the well-established p-type TCOs. However, as processed CuI loses its transparency and conductivity with time in an ambient condition which makes them unsuitable for long term applications. Herein, we propose CuI-TiO_2 composite thin films as a replacement of pure CuI. We show that the introduction of TiO_2 in CuI makes it more stable in ambient condition while also improving its conductivity and transparency. A detailed comparative analysis between CuI and CuI-TiO_2 composite thin films have been performed to understand the reasons for improved conductivity, transparency and stability of CuI-TiO_2 samples in comparison to pure CuI samples. The enhanced conductivity in CuI-TiO_2 stems from the space-charge layer formation at the CuI/TiO_2 interface, while the improved transparency is due to reduced CuI grain growth mobility in the presence of TiO_2. The improved stability of CuI-TiO_2 in comparison to pure CuI is a result of inhibited recrystallization and grain growth, reduced loss of iodine and limited oxidation of CuI phase in presence of TiO_2. For optimized fraction of TiO2, average transparency of ~78% (in 450-800 nm region) and a resistivity of 14 mΩ.cm is achieved, while maintaining a relatively high mobility of ~3.5 $cm^2V^{-1}s^{-1}$ with hole concentration reaching as high as 1.3 x 10^{20} cm^{-3}. Most importantly, this work opens up the possibility to design a new range of p-type transparent conducting materials using CuI/insulator composite system such as CuI/SiO_2, CuI/Al_2O_3, CuI/SiN_x, etc.

INTRODUCTION

Transparent conductors (TCs) are a class of materials that display close to metal conductivity (~10^3

- 10^4 S cm^{-1}) while maintaining high transparency (> 80 %) in the visible region.[1-2] TCs have widely been used for applications in solar cells, LEDs, transistors, thermoelectrics, etc. [1-2] Commonly used TCs are heavily doped n-type wide-bandgap semiconductors such as In_2O_3, SnO_2, ZnO and GaN, whereas, high-performance p-type TCs are not very well developed. [1, 3] Nonetheless, Cu^+-based oxides such as delafossite $CuMO_2$ (M: Al^{3+}, Ga^{3+}, In^{+3}, Sc^{3+}, Y^{3+}) have been widely investigated as p-type TCs but are unable to match the performance of n-type TCs in terms of conductivity and transparency.[3-10] Most recently, $La_{2/3}Sr_{1/3}VO_3$, a Mott–Hubbard insulator has been reported to achieve a high conductivity of 742.3–872.3 S cm^{-1}, however, the transparency of a 48 nm-thick film remains limited to ~55 % in the visible region.[11] Also, these p-type transparent conducting oxides need high processing temperature (> 400 ^oC) which makes them unsuitable for organic and/or flexible electronics. Consequently, a high-performance p-type TC that can be synthesized and doped at low temperature while maintaining high-conductivity and high optical transmittance is extremely desirable for both active and passive electronic applications.

Copper iodide (CuI) is a p-type wide band gap semiconductor with a fairly small effective mass of $0.30m_0$ for light holes and a bulk mobility of >40 $cm^2V^{-1}s^{-1}$.[12] Even for CuI thin films, mobilities of 8-20 $cm^2V^{-1}s^{-1}$ have readily been reported.[13-16] Furthermore, CuI can be synthesized and heavily doped at low temperatures (<100 ^oC) to achieve a hole conductivity of σ > 280 S/cm while maintaining a transparency of more than 70%.[14-15, 17] Owing to aforementioned qualities, CuI has been used to achieve high solar cell efficiencies,[18-22] high rectification ratio diodes (rectification ratios larger than 10^9),[23-24] photodetectors,[25] piezoelectric enhancement,[26] flexible transparent thin film transistors (TFTs),[27] and light emitting diodes[28-29]. In addition, CuI has most recently been used as a transparent thermoelectric material to achieve a large thermoelectric figure

of merit of ZT=0.21 at 300 °C, which is three orders of magnitude higher compared with state-of-the-art p-type transparent materials. [14, 30-31] The above-mentioned striking advantages make CuI an important material for device applications.

However, γ-CuI deposited using different techniques have been found to be unstable in ambient conditions because of recrystallization, grain growth, loss of iodine and unwanted oxidation,[24, 32-35] which can significantly reduce its transparency and conductivity over time. To achieve long-term stability in ambient condition, stabilization of CuI at individual grain level is required and yet there are very few reports investigating this issue. In 1963, Herrick et al had shown that the composite of CuI with Cu_2O can significantly improve the stability while maintaining or even improving the conductivity and transparency of pure CuI. [32, 36] However, the authors did not perform any detailed investigation to show the reasons for these improvements. Nonetheless, there are several reports on improving the conductivity of metal halides through the introduction of metal oxides. [33-36]

Liang, in 1973 first observed an enhancement of up to three orders of magnitude in the conductivity of LiI upon addition of Al_2O_3 particles.[37] He deduced that the Li^+ ions are adsorbed onto the LiI/Al_2O_3 interface, thereby increasing the Li vacancy concentration in LiI by orders of magnitude which leads to significant increase in conductivity. [37-40] Since then, Li-, Cu-, Ag-, Na-, Cd-, Cs- and Tl-halides have been doped with metal oxides such as Al_2O_3, TiO_2, SiO_2, Fe_2O_3, $BaTiO_3$, ZrO_2, CeO_2, to enhance their conductivity. [37-38, 41-45]

Herein, we show that the addition of TiO_2 into CuI significantly enhances its stability, hole conductivity and transparency. Structural and optical characterizations performed using X-Ray diffraction (XRD) and Raman show no new peaks for CuI-TiO_2 when compared to pure CuI. However, a distinctive change in morphology is confirmed by field-emission scanning electron

microscopy (FESEM). Furthermore, the mechanisms for increased conductivity, transparency and stability are discussed and substantiated using different characterization techniques such as FESEM, conductive atomic force microscopy (C-AFM), energy-dispersive X-ray spectroscopy (EDS) and cathodoluminescence (CL).

MATERIALS AND METHODS

Sample synthesis started with the deposition of a copper thin film with and without TiO_2 on 2.5 cm x 2.5 cm glass slides in an ATC 1800 UHV sputter deposition system using 99.99 % pure targets. For CuI, the copper film was deposited using DC sputtering at 50 W power. For CuI-TiO_2, TiO_2 target was co-sputtered with varying RF powers from 60 to 180 W to vary the TiO_2 concentration. The DC power to copper target was similar to that used to prepare CuI. All sputter depositions were performed in an argon only environment at a pressure of 1.5 mTorr with an argon flow of 10 sccm. The glass slides with the films were then transferred into a petri dish and covered with 100 grams of iodine beads. Subsequently, the petri dish containing the glass slides and iodine was sealed using parafilm. Both Cu and Cu-TiO_2 thin films become transparent after an hour of iodine exposure at room temperature. It is important to note that the final thickness of CuI was almost 7 times the original thickness of copper film because of volume expansion. To further dope the CuI and CuI-TiO_2 films, the samples were left for another 48 hours in a saturated iodine atmosphere at room temperature. It has been shown experimentally that iodine vapor can increase the hole concentration in CuI samples by incorporation of iodine into the crystal lattice.[46-47] This reaction can be written as:

$$CuI\ (s) + \frac{1}{2}\ I_2\ (g)\ \rightleftarrows CuI\ (s) + \ I_I^x + \ V_{Cu}' + \ h^{\cdot}$$

where, $I_I^{\times}$ denotes an iodine ion sitting at iodine lattice site with neutral charge, $and\ V'_{Cu}$and $h^{\cdot}$ denote the copper cation vacancy and the corresponding hole, respectively. These heavily doped CuI and CuI-TiO_2 samples were then rinsed in IPA/acetone until the surface iodine was totally removed. Based on the power used for TiO_2 sputtering, we name our samples as CuI-TiO_2-60, CuI-TiO_2-120, and CuI-TiO_2-180, respectively, where the numbers at the end denote the RF power used for TiO_2 co-deposition. The final thickness for all samples was ~270 ± 20 nm.

The transmittance and reflectance of CuI and CuI-TiO_2 thin films were measured using a Shimazdu UV-Visible-IR spectrophotometer in the wavelength range of 300-1800 nm. Room temperature Hall effect measurements were performed using a Lakeshore Hall effect measurement system, at magnetic fields varying from -10 to + 10 kG with a step size of 2 kG. Furthermore, to better understand the effect of TiO_2 on CuI thin films, several of other characterizations were performed such as FESEM (Field Emission Scanning Electron Microscope), grazing incidence XRD (X-ray diffraction), Raman, EDS (Energy-dispersive X-ray spectroscopy) and secondary ion mass spectroscopy (SIMS). FESEM measurements were performed using an FEI Verios system, whereas GIXRD measurements were performed using ESCALAB 250Xi XRD system from Thermo Scientific. Raman spectra of the films were measured using Horiba's JOBIN YVON spectrometer with a 532 nm excitation source. SIMS measurements were performed using an IMS 5fE7 instrument (Cameca, France). A primary ion beam of Cs^+ with an impact energy of 5.0 keV and beam current of 3 nA was employed to raster a 180 μm × 180 μm region of the surface. Positive secondary ions were accepted from a circular area limited to a diameter of 33 μm by ion optical aperture in order to avoid crater effects. For each crater, the total depth of the crater, measured by a KLA Tencor Alpha-Step IQ profilometer (KLA-Tencor, U.S.A.), was used to calculate the average ion beam sputter rate necessary for converting the SIMS analysis time into depth profile.

Finally, Conductive Atomic Force Microscopy (C-AFM) and cathodoluminescence (CL) measurements were performed to investigate the mechanism of improved conductivity and stability, respectively. C-AFM measurements were conducted in air by a Cypher AFM (Asylum Research, Oxford). Current mapping was obtained by the Asylum Research ORCA cantilever holder with dual gain (sensitivity: 1 nA/V and 1 µA/V; current range: ±10 nA and ±10 µA). Conducting Pt/Ir-coated silicon probe (Nanosensor, PPP-EFM) with a calibrated spring constant ~ 1.67 nN/nm was employed for all the C-AFM measurements. CL measurements were performed using an FEI Verios 460 FESEM equipped with a Gatan MonoCL4 Elite CL system with 5 kV beam voltage and 0.2 nA beam current.

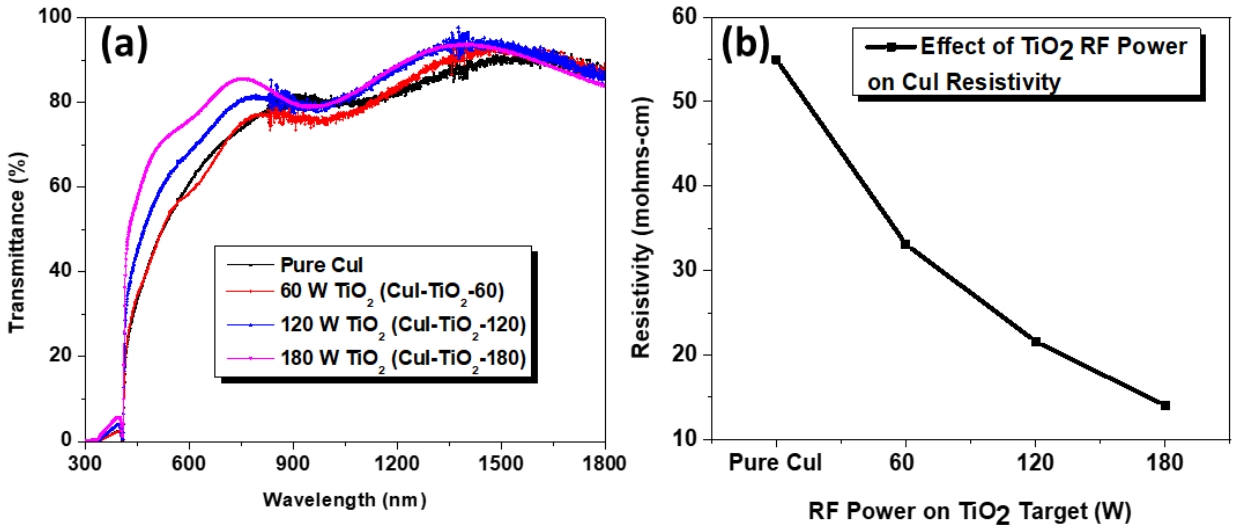

Figure 1. Effect of TiO_2 RF power on the (a) transmittance of CuI-TiO_2 samples, and (b) resistivity of the different CuI-TiO_2 composite samples. The pure CuI sample is also shown for comparison.

RESULTS AND DISCUSSION

The effect of TiO_2 power on the transparency and resistivity of CuI-TiO_2 samples is shown in Figure 1(a) and 1(b), respectively. It is quite evident that introduction of TiO_2 can significantly

improve the transparency of CuI thin films, especially in the visible regime (400 – 800 nm). As will be shown later, the increased transparency of CuI-TiO_2 samples in comparison to pure CuI sample could be explained in terms of Zener pinning which inhibits the grain growth and therefore reduces the roughness of the CuI-TiO_2 samples leading to reduced scattering of light and increased transparency. The average transmittance of CuI-TiO_2-180 sample is significantly improved to ~78% in 450 – 800 nm regime in comparison to pure CuI, average transmittance of which is ~61% in the same regime.

The resistivity of CuI and CuI-TiO_2 samples are shown in Figure 1(b). A decrease in resistivity of CuI-TiO_2 samples with increased power of TiO_2 deposition (increased concentration of TiO_2) follow almost linear curve. Similar results have been reported both experimentally and theoretically for other metal halides doped with oxides. [37-38, 41-42, 44-45] Amongst all measured samples, the lowest resistivity was obtained for CuI-TiO_2-180 samples. For CuI-TiO_2-180 samples, a resistivity of ~14 mΩ.cm is obtained while the resistivity of pure CuI prepared under similar condition was ~56 mΩ.cm. A decrease in CuI resistivity with TiO_2 incorporation is mainly because of increased hole density, which increases from $4x10^{19}$ cm^{-3} for pure CuI to $1.3x10^{20}$ cm^{-3} for CuI-TiO_2 samples, as confirmed by Hall effect measurements (see Figure S2). In addition, incorporation of TiO_2 also increases the Hall mobility of CuI samples from 2.75 to 3.5 $cm^2V^{-1}s^{-1}$, most likely due to increased grain packing density and increased grain boundary conductivity, both of which favors the charge transport within the grain boundaries. This effect will be explained in later part of this section by assuming the formation of a space charge layer at the CuI/TiO_2 interface.

For simplicity, here onwards, we only compare the results of pure CuI and CuI-TiO_2-180 samples to explain reasons for improved conductivity, transparency and stability of CuI with the

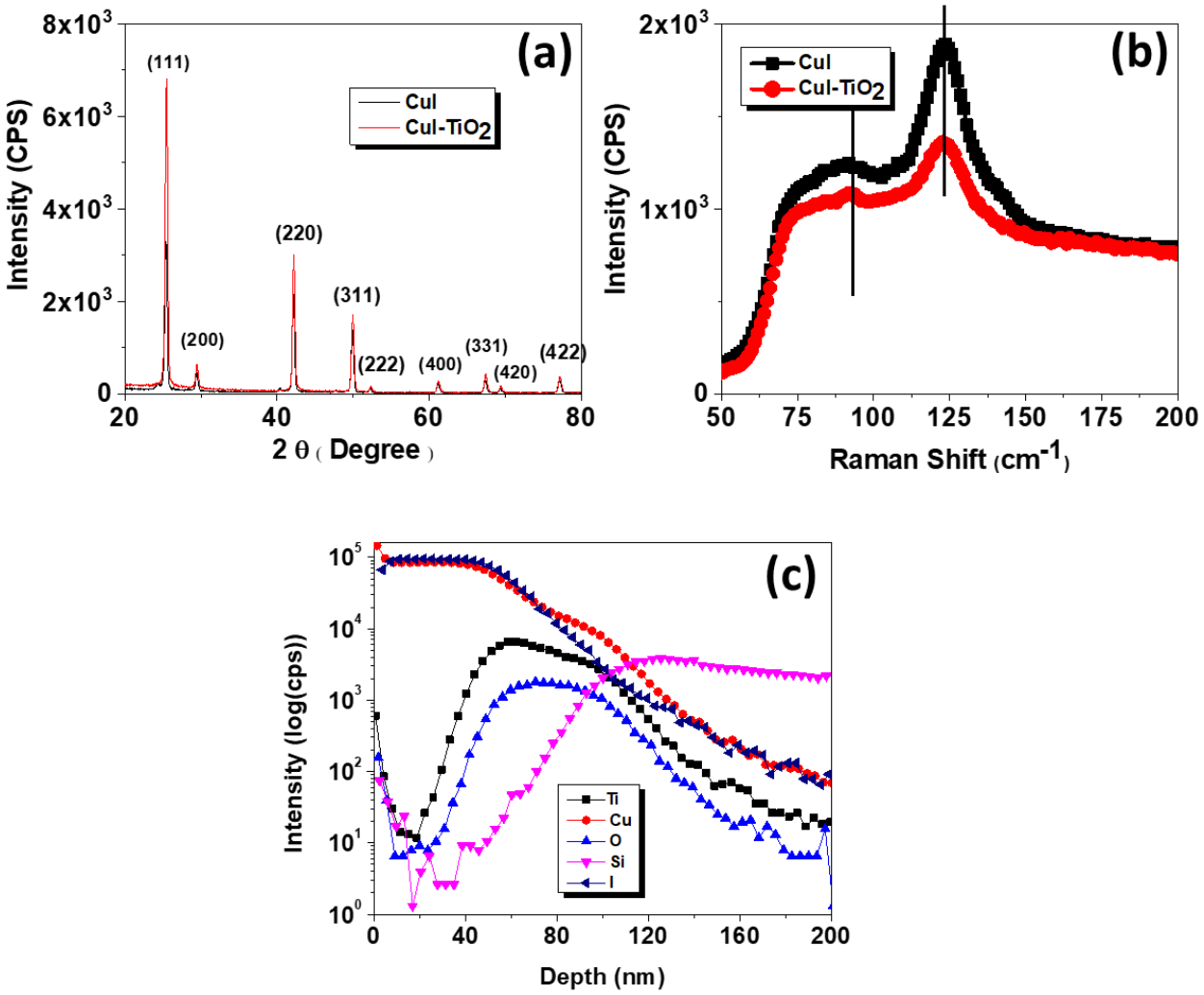

Figure 2. Comparative XRD diffraction patterns (a), and Raman spectra (b) for CuI and CuI-TiO_2-180 samples. (c) SIMS profiles of CuI-TiO_2-180 showing the depth profile of various elements.

introduction of TiO_2. The XRD patterns for CuI and CuI-TiO_2-180 samples are shown in figure 2(a). It is unambiguous that no additional peak can be detected for CuI-TiO_2 sample, suggesting the addition of TiO_2 does not introduce any crystalline phases. This observation is consistent with previously reported results where insulating oxides such as Al_2O_3, SiO_2, TiO_2 were used to improve the conductivity of metal halides such as LiI, $CuCl_2$, AgI without any new phase detectable by XRD. [38] An absence of any characteristic peaks of TiO_2 in XRD is because it exists in an

amorphous phase as confirmed by electron diffraction pattern shown in figure S4 of the supplementary section. Both CuI and CuI-TiO_2-180 samples show (111) as the preferred crystal orientation, since (111) planes in zincblende CuI have the minimum surface energy and the fastest growth rate [12, 23]. XRD pattern for both CuI and CuI-TiO_2-180 samples confirm the formation of pure fcc γ-CuI as confirmed by JCPDS 2.00 card No. 06-0246.

Figure 2(b) shows the Raman spectra for the CuI and CuI-TiO_2-180 samples. Similar to XRD; Raman measurements were not able to detect any significant difference between the two samples. The Raman spectra for both CuI and CuI-TiO_2-180 samples show very well resolved peak at ~124 cm^{-1} corresponding to transverse optical mode (TO), whereas a smaller peak at lower wavenumber (~90 cm^{-1}) corresponds to transverse acoustic mode.

SIMS profiles for different elements detected in CuI-TiO_2-180 are shown in Figure 3(c). It is quite clear from Figure 3(c) that TiO_2 is present in the CuI-TiO_2 sample with a more pronounced TiO_2 incorporation towards the bottom of the layer, which is in agreement with EDS measurement performed on the same sample (see Figure S3 of the supplementary section). The quantitative analysis of TiO_2 in CuI was performed against a standard implanted sample with known concentration of Ti and O in CuI. The calculated peak concentration of TiO_2 in the sample is ~$1x10^{21}$ cm^{-3} which corresponds to ~5 atomic percent.

FESEM images of CuI and CuI-TiO_2-180 are shown in Figure 3(a-c) and 3(d-f), respectively. It is quite apparent that CuI in absence of TiO_2 tends to form bigger grains which increase the scattering of incoming light and gives a milky appearance. Furthermore, for films with thickness of only few hundred nanometers, these large grains tend to aggregate with each other in a random fashion leaving behind empty spaces between aggregates which further reduces the transparency of pure CuI thin films because of increased scattering. On the other hand, the use of TiO_2 reduces the grain

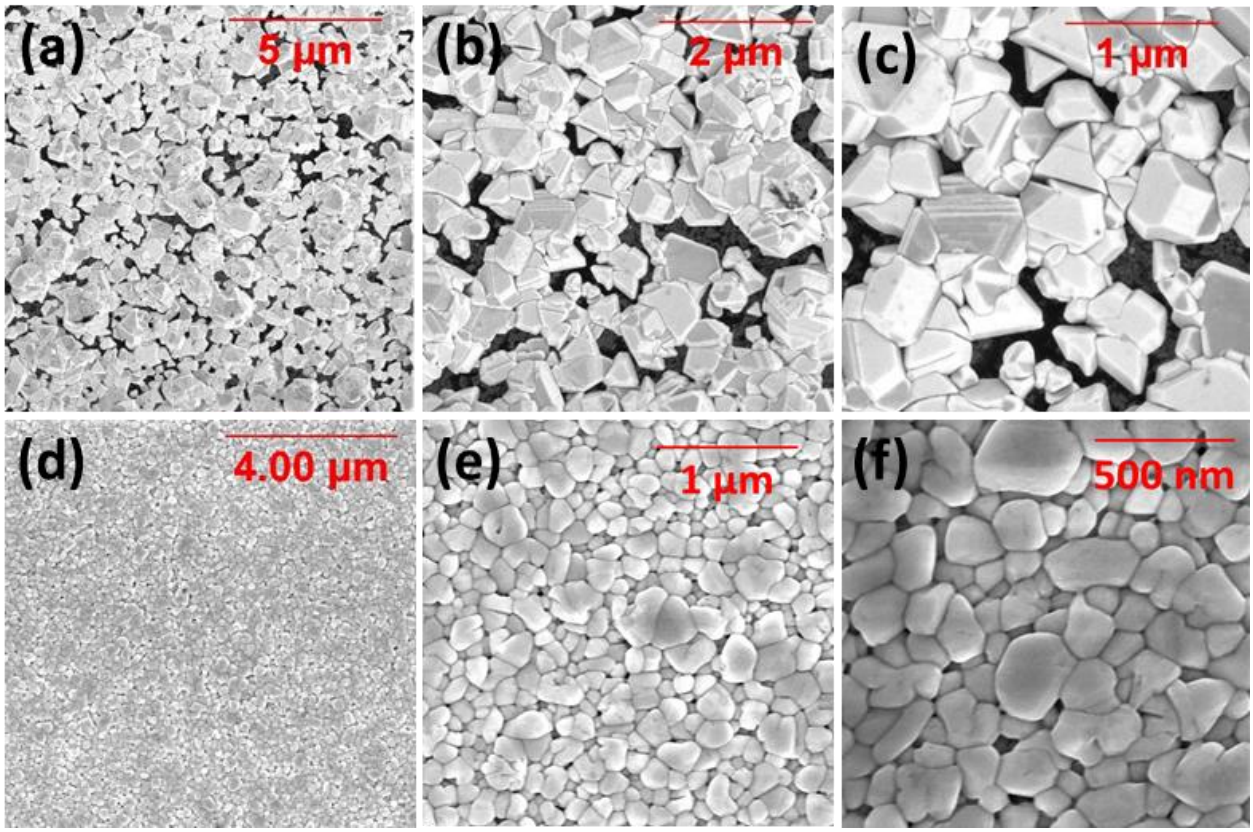

Figure 3. (a-c) FESEM images of CuI sample shown at different magnifications. Smaller grains aggregate with each other to form bigger clusters leaving empty spaces in between which cause scattering of light and a milky appearance in CuI samples. (d-f) FESEM image of CuI +TiO_2-180 samples at different magnifications. In contrast to CuI sample, CuI+TiO_2-180 grains tend to form a closely packed clusters and relatively smooth surface, which in turn leads to higher transparency.

size (see Figure 3(d-f)) and the smaller grains form a more compact thin film structure which minimizes the scattering of light and thus reduces the milky appearance and increases the transmittance of light. Previously, second phase materials have often been employed to inhibit the grain growth, especially in polycrystalline metals and ceramics. [48-54] It has been reported that grain mobility can be significantly influenced in the presence of second phase particles,[48-51] which act as obstacles to the motion of grain boundaries and thus retard grain growth.[51] Smith and Zener

were the first to study the effect of volume fraction (*f*) of second phase material on the abnormal grain growth of polycrystalline materials.[52-53] They deduced that in the presence of a spherical second phase particle with diameter (*d*) and volume fraction (*f*), the stabilized grain size (D_{max}) of the polycrystalline material is directly proportional to *d* and inversely proportional to *f*. Though some fine tuning to this model have been made by several other researchers,[54] it remains the fact that increased volume fraction of second phase material decreases the size of the stabilized grain.[50, 54] In the current scenario, increasing the TiO_2 concentration decreases the grain size of polycrystalline CuI leading to a reduced light scattering and increased transmission. The presence

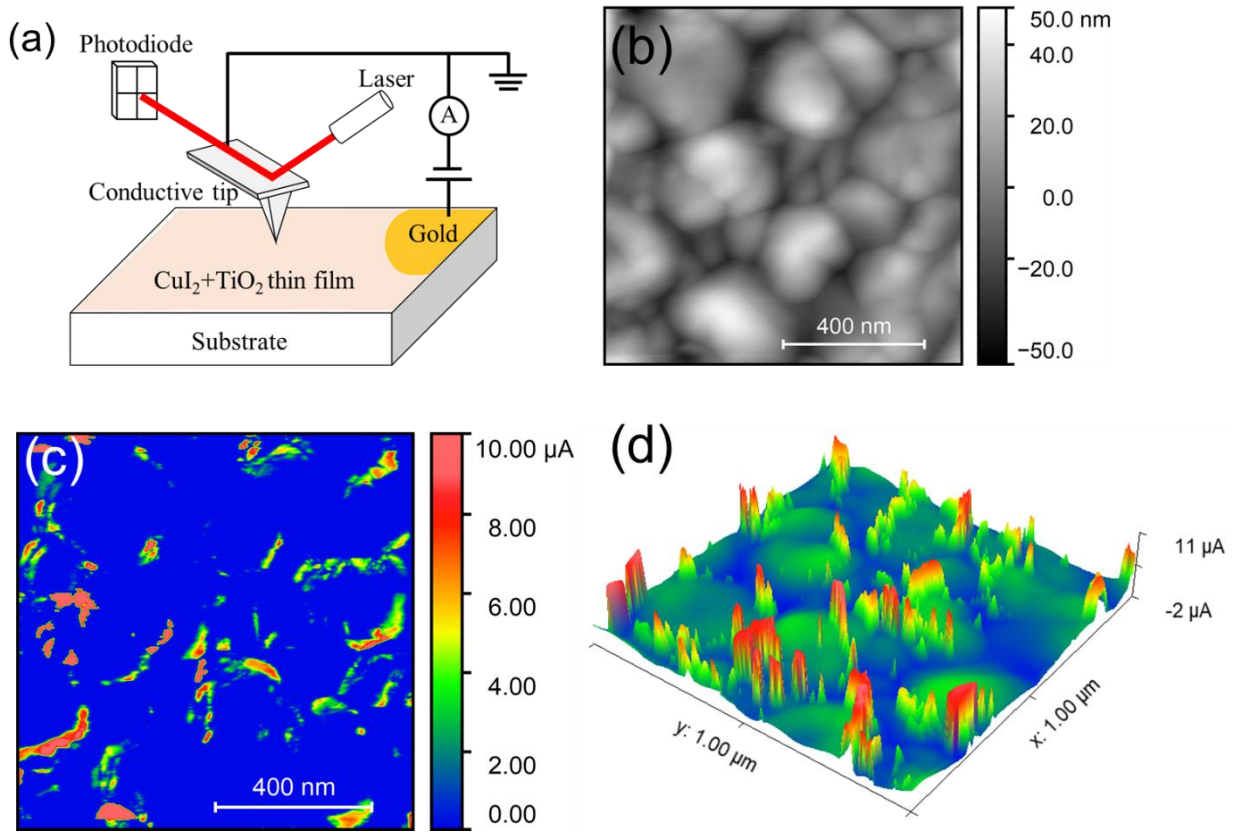

Figure 4. (a) Schematic of the set-up for the C-AFM. (b) The morphology of a 1 µm × 1 µm region of the CuI-TiO_2 film and (c) corresponding current mapping over the same area. (d) Three-dimensional representation of the current map overlaid on the morphology contour.

of TiO_2 in CuI is further confirmed by EDS measurements on CuI-TiO_2 samples shown in Figure S3 of the supplementary section.

There are several different mechanisms to explain the enhanced conductivity in metal halides by the inclusion of an insulating phase. [38-39, 41-42, 55-57] Though different theories take different routes, all of them reaches to the same conclusion that interfaces play a major role in the conductivity enhancement of these mixed phase conductors. Maier's theory is one of the most accepted theory which supports the formation of a highly conductive space-charge layer at the interface of CuI/TiO_2[38, 57-60] To experimentally verify the formation of highly conductive space charge region at the CuI/TiO_2 interface, we performed the conductive AFM measurements.

Figure 4a shows the schematic diagram of the set-up for C-AFM. Figure 4b is the morphology of the CuI-TiO_2-180 thin film with a 1 μm × 1 μm scanning area collected in contact mode (contact force ~ 25 nN). The black and white contrast indicates the height differences. The grain size typically ranges from 80 to 300 nm, which is in accordance with the SEM measurement. Figure 4c presents the current scanned in the same region shown in Figure 4b under a DC bias of 500 mV. To better visualize the current distribution, the current image is overlaid on the corresponding morphology image and plotted in 3-D rendition (Figure 4d). As predicted by theory, the interfaces of CuI-TiO_2-180 samples show significantly higher conductivity as compared to bulk regions. Figure 4d further corroborates that the flow of charges are mainly at the grain boundaries, which confirms the enhancement of conductivity at the interfaces. C-AFM measurements were also performed on pure CuI samples (shown in Figure S6 of the supplementary section) under similar conditions (at same voltage). However, no significant current flow was detected around the grain boundaries in pure CuI samples.

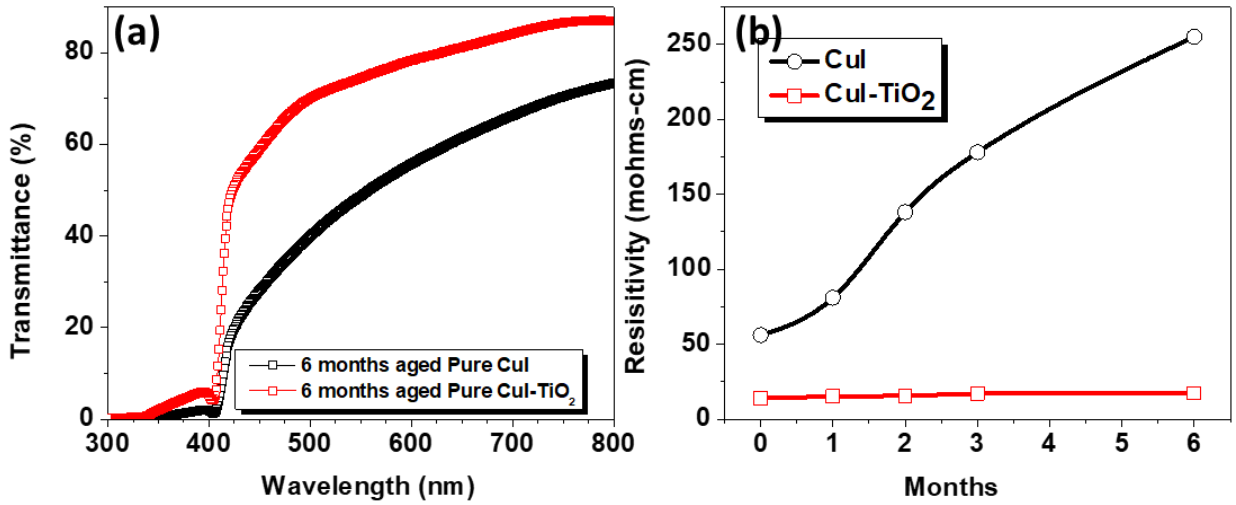

Figure 5. (a) UV-Vis spectra for CuI and CuI-TiO_2 samples aged for 6 months at ambient condition. (b) Effect of ageing on resistivity of CuI and CuI-TiO_2 samples.

Further, it is well known that the electronic and optical properties of CuI can degrade significantly when stored in ambient condition for long durations.[24, 32-33, 36] Therefore, we monitor the optical transmittance and the conductivity of both CuI and CuI-TiO_2-180 samples left in ambient condition over a duration of 6 months. The UV-Vis spectra for CuI and CuI-TiO_2-180 samples after 6-months storage are shown in Figure 5(a). It is quite evident that the transparency of CuI-TiO_2-180 sample shows no appreciable change (compare Figure 5(a) and 2(a)), whereas, the average transparency of pure CuI reduces to below 50% in the 400-800 nm regime. Similar to optical transparency, the electronic behavior of CuI (shown in Figure 5(b)) also degrades with ageing and the resistivity of CuI samples increases from ~56 to ~260 mΩ.cm, over a duration of 6 months. However, under similar conditions, the resistivity of CuI-TiO_2-180 samples (Figure 5(b)), remains within ± 5% of the original value i.e. ~14 mΩ.cm. These results confirm that the Introduction of TiO_2 in CuI not

only improves its optical transparency and holes conductivity but also increases its stability in ambient condition.

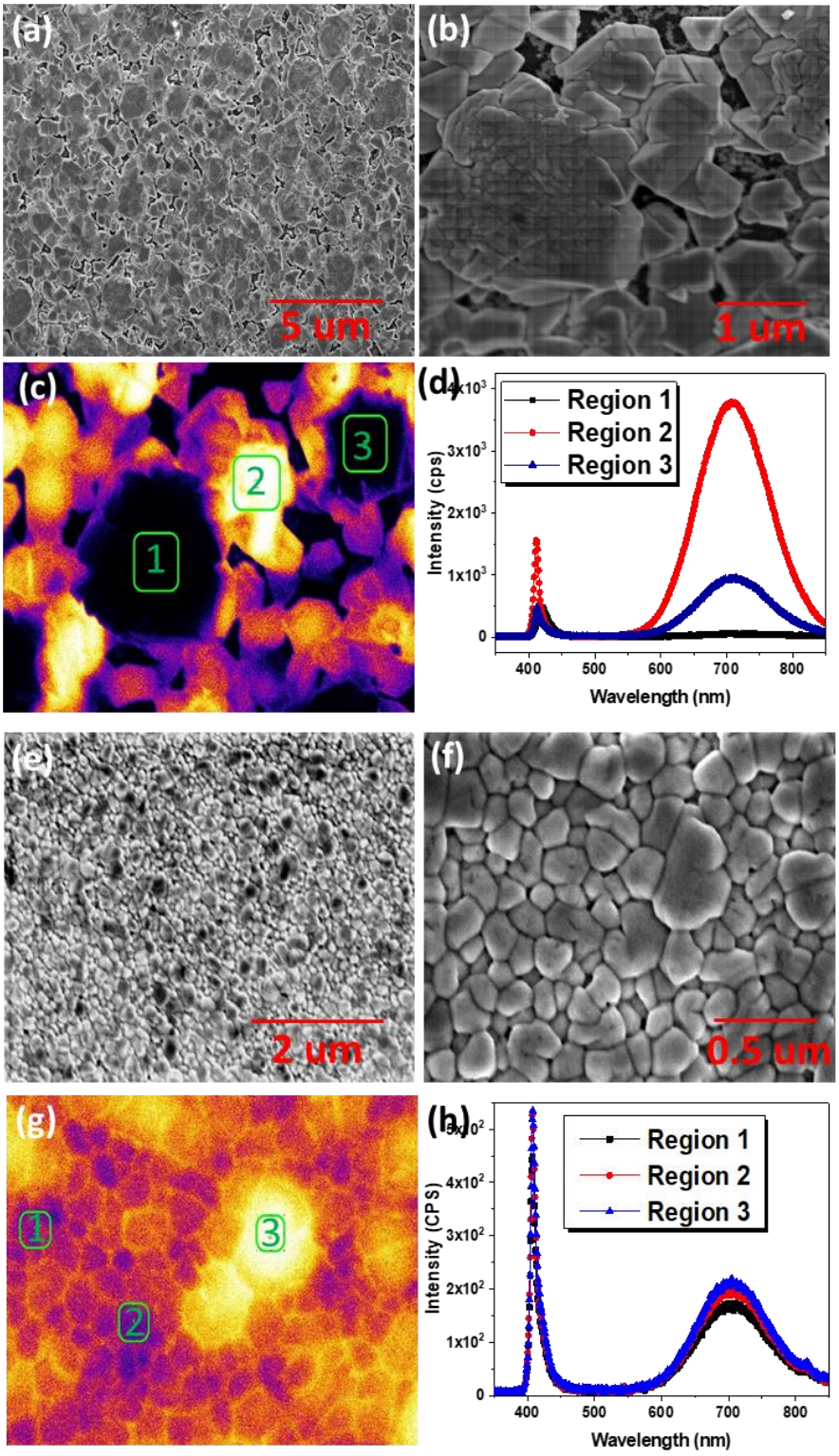

Figure 6. (a) and (b) shows the SEM of a CuI sample after ageing for 6 months. Comparing the SEM of fresh sample and aged sample (Figs 2a-c), the change in morphology of larger grains is quite apparent. (c) Panchromatic CL mapping of an aged CuI sample. Three different regions (in green boxes) were selected to perform spectral analysis. (d) CL spectra from three different regions. (e) and (f) shows a CuI-TiO_2-180 sample after ageing for 6 months. No significant change in the morphology of grains was visible when compared to a freshly prepared CuI-TiO_2-180 sample (Figs 2d-f). (g) Panchromatic `CL mapping of an aged CuI-TiO_2-180 sample. Three different regions marked by the green boxes are spectrally analyzed, the results of which are shown in (h).

Previously, it has been postulated that degradation of CuI samples with time is because of recrystallization, grain growth, loss of iodine and unwanted oxidation of CuI.[32] Therefore, to better understand the reason for improved stability of CuI-TiO_2-180 in comparison to pure CuI samples, combined SEM-CL measurements were performed on aged CuI and CuI-TiO_2-180 samples. It is quite apparent from the images that the grains in aged pure CuI (Figure 6(a-b)) have grown large and rough over time, most probably due to re-crystallization and discontinuous grain growth, leading to increased light scattering and decreased transparency. In contrary, grains of aged CuI-TiO_2-180 (Figure 6(e, f)) show no distinct change in the morphology and remain a continuous and relatively smooth layer. As discussed earlier, TiO_2 might be reducing the grain boundary mobility by segregating at the grain boundaries leading to inhibited grain growth. Though not very common for halides, impurities have often been used to inhibit the grain growth in metals [61-62] oxides, [63-64] and other polycrystalline films [50-51, 54] to reduce degradation over time. In addition, the concept of segregation of TiO_2 at the grain interface agrees well with the increased interface conductivity in CuI-TiO_2-180 samples as confirmed by C-AFM measurement (Figure 4).

In addition to FESEM analysis, we also perform a cathodoluminescence (CL) analysis to investigate the chemical changes that might be happening at the grain level in aged CuI and CuI-TiO_2-180 samples. The panchromatic CL images for aged pure CuI and CuI-TiO_2-180 samples are shown in Figure 6(c) and 6(g), respectively. To analyze the CL results in both CuI and CuI-TiO_2-180 samples, we mark three different regions and plot the corresponding CL spectrum for these regions in Figure 6(d) and Figure 6(h) for CuI and CuI-TiO_2-180 samples, respectively. Both CuI and CuI-TiO_2-180 samples show a sharp peak at lower wavelength, and a wider peak in 600-800 nm wavelength regime. The sharp peak at lower wavelength (at ~410 nm) corresponds to band-to-band recombination, whereas the wider peak in 600-800 nm wavelength regime corresponds to defects due to iodine vacancy (at ~690 nm) and oxidation of CuI (at ~750 nm).[65-66] Though both CuI and CuI-TiO_2-180 show very high luminescence in panchromatic CL image shown in Figure 6 (c) and 6(g), respectively, it is important to note that the luminescence in pure CuI is dominated by defect recombination, whereas the luminescence in CuI-TiO_2-180 samples is dominated by band-to-band recombination. This is important because the loss of electronic conductivity of CuI with time has previously been attributed to oxidation and loss of iodine, for which the defect-based luminescence is detected in the 600-800 nm regime.[32-33, 36, 67] In general, for CuI defect peak consists of two different peaks; one at ~690 nm and the other one at ~750 nm. The peak at ~690 nm corresponds to iodine vacancies in CuI samples, whereas, the second peak at ~750 nm can be ascribed to oxygen vacancies, which results from the oxidation of I^- ions.[68-71] It is quite evident from comparison of Figure 6(d) and 6(h) that CuI-TiO_2-180 did not oxidize or lost iodine as badly as pure CuI. This agrees with the fact that CuI-TiO_2-180 shows better ambient stability in comparison to pure CuI.

CONCLUSION

In conclusion, we have shown that the optical and electronic characteristics of CuI can be significantly improved through the incorporation of TiO_2. TiO_2 helps to achieve size and stability of individual CuI grains which in turn improves their stability, and consequently the conductivity and transparency of the film. Though no new XRD, or Raman peaks have been detected for CuI-TiO_2 samples in comparison to pure CuI samples; SIMS and EDS analysis confirm the distribution of TiO_2 in CuI samples. In addition, FESEM confirms that TiO_2 can inhibit grain growth and recrystallization of CuI. C-AFM measurement shows high conductivity at the grain interfaces of CuI-TiO_2-180 sample in comparison to pure CuI grain interfaces, which confirms the hypothesis of the formation of highly conductive region at the CuI/TiO_2 interface. Such enhanced conductivity at the CuI/TiO_2 interface is the major reason for higher bulk conductivity in CuI-TiO_2 samples as compared to pure CuI samples. Moreover, a comparative SEM-CL measurement on aged CuI and CuI-TiO_2 samples, show that pure CuI loses transparency and conductivity because of recrystallization, grain growth, loss of iodine and unwanted oxidation. In comparison, CuI-TiO_2 samples do not show any significant change and maintains its stability. Finally, it is expected that this work will become basis for achieving a CuI based p-type transparent conductor with high transparency, conductivity and ambient stability.

ASSOCIATED CONTENT

Supporting Information. An electronic copy of the supporting information is available online or from the author.

AUTHOR INFORMATION

Corresponding Author

Vidur.raj@anu.edu.au

Author Contributions

The manuscript was written through contributions of all authors. All authors have given approval to the final version of the manuscript.

Funding Sources

This research is funded by Australian Research Council.

ACKNOWLEDGMENT

This research is supported by the Australian Research Council. The Australian National Fabrication Facility (ANFF) and Australian Microscopy and Microanalysis Research Facility (AMMRF) is gratefully acknowledged for providing access to the fabrication and microscopy facilities used in this work. YL and TL thanks the financial support from Australian Research Council in the form of discovery project (DP160104780).

REFERENCES

(1) Hautier, G.; Miglio, A.; Ceder, G.; Rignanese, G. M.; Gonze, X. Identification and design principles of low hole effective mass p-type transparent conducting oxides. *Nature Communications* **2013,** *4*, 1-7, DOI: 10.1038/ncomms3292.
(2) Zhang, K. H. L.; Xi, K.; Blamire, M. G.; Egdell, R. G. P -type transparent conducting oxides. *Journal of Physics: Condensed Matter* **2016,** *28* (38), 383002-383002, DOI: 10.1088/0953-8984/28/38/383002.
(3) Klein, A. Transparent conducting oxides: Electronic structure-property relationship from photoelectron spectroscopy with in situ sample preparation. *Journal of the American Ceramic Society* **2013,** *96* (2), 331-345, DOI: 10.1111/jace.12143.
(4) Zhang, K. H. L.; Du, Y.; Papadogianni, A.; Bierwagen, O.; Sallis, S.; Piper, L. F. J.; Bowden, M. E.; Shutthanandan, V.; Sushko, P. V.; Chambers, S. A. Perovskite Sr-Doped LaCrO ₃ as a New p-Type Transparent Conducting Oxide. *Advanced Materials* **2015,** *27* (35), 5191-5195, DOI: 10.1002/adma.201501959.

(5) Duan, N.; Sleight, A. W.; Jayaraj, M. K.; Tate, J. Transparent p-type conducting CuScO2+x films. *Applied Physics Letters* **2000,** *77* (9), 1325-1325, DOI: 10.1063/1.1289906.
(6) Ueda, K.; Hase, T.; Yanagi, H.; Kawazoe, H.; Hosono, H.; Ohta, H.; Orita, M.; Hirano, M. Epitaxial growth of transparent p-type conducting CuGaO[sub 2] thin films on sapphire (001) substrates by pulsed laser deposition. *Journal of Applied Physics* **2001,** *89* (3), 1790-1790, DOI: 10.1063/1.1337587.
(7) Yanagi, H.; Hase, T.; Ibuki, S.; Ueda, K.; Hosono, H. Bipolarity in electrical conduction of transparent oxide semiconductor CuInO2 with delafossite structure. *Applied Physics Letters* **2001,** *78* (11), 1583-1585, DOI: 10.1063/1.1355673.
(8) Sarmadian, N.; Saniz, R.; Partoens, B.; Lamoen, D. Easily doped p-type, low hole effective mass, transparent oxides. *Scientific Reports* **2016,** *6* (January), 1-9, DOI: 10.1038/srep20446.
(9) Lunca Popa, P.; Crêpellière, J.; Nukala, P.; Leturcq, R.; Lenoble, D. Invisible electronics: Metastable Cu-vacancies chain defects for highly conductive p-type transparent oxide. *Applied Materials Today* **2017,** *9*, 184-191, DOI: 10.1016/j.apmt.2017.07.004.
(10) Jayaraj, M. K.; Draeseke, A. D.; Tate, J.; Sleight, A. W. p-Type transparent thin films of CuY1−xCaxO2. *Thin Solid Films* **2001,** *397* (1-2), 244-248, DOI: 10.1016/S0040-6090(01)01362-1.
(11) Hu, L.; Wei, R.; Yan, J.; Wang, D.; Tang, X.; Luo, X.; Song, W.; Dai, J.; Zhu, X.; Zhang, C.; Sun, Y. La _{2/3} Sr _{1/3} VO ₃ Thin Films: A New p-Type Transparent Conducting Oxide with Very High Figure of Merit. *Advanced Electronic Materials* **2018,** *4* (3), 1700476-1700476, DOI: 10.1002/aelm.201700476.
(12) Grundmann, M.; Schein, F. L.; Lorenz, M.; Böntgen, T.; Lenzner, J.; Von Wenckstern, H. Cuprous iodide - A p-type transparent semiconductor: History and novel applications. *Physica Status Solidi (A) Applications and Materials Science* **2013,** *210* (9), 1671-1703, DOI: 10.1002/pssa.201329349.
(13) Yamada, N.; Ino, R.; Ninomiya, Y. Truly Transparent p-Type γ-CuI Thin Films with High Hole Mobility. *Chemistry of Materials* **2016,** *28* (14), 4971-4981, DOI: 10.1021/acs.chemmater.6b01358.
(14) Yang, C.; Souchay, D.; Kneiß, M.; Bogner, M.; Wei, H. M.; Lorenz, M.; Oeckler, O.; Benstetter, G.; Fu, Y. Q.; Grundmann, M. Transparent flexible thermoelectric material based on non-toxic earth-abundant p-type copper iodide thin film. *Nature Communications* **2017,** (May), in press-in press, DOI: 10.1038/ncomms16076.
(15) Yamada, N.; Ino, R.; Tomura, H.; Kondo, Y.; Ninomiya, Y. High-Mobility Transparent p-Type CuI Semiconducting Layers Fabricated on Flexible Plastic Sheets: Toward Flexible Transparent Electronics. *Advanced Electronic Materials* **2017,** *3* (12), 1700298-1700298, DOI: 10.1002/aelm.201700298.
(16) Yang, C.; Kneiβ, M.; Lorenz, M.; Grundmann, M. Room-temperature synthesized copper iodide thin film as degenerate p-type transparent conductor with a boosted figure of merit. *Proceedings of the National Academy of Sciences of the United States of America* **2016,** *113* (46), 12929-12933, DOI: 10.1073/pnas.1613643113.
(17) Amalina, M. N.; Rusop, M. In *The properties of P-type copper (I) iodide (CuI) as a hole conductor for solid-state dye sensitized solar cells*, 2013/09//; IEEE: pp 300-303.
(18) Das, S.; Choi, J.-Y.; Alford, T. L. P3HT:PC61BM based solar cells employing solution processed copper iodide as the hole transport layer. *Solar Energy Materials and Solar Cells* **2015,** *133*, 255-259, DOI: 10.1016/j.solmat.2014.11.004.

(19) Wang, H.; Yu, Z.; Jiang, X.; Li, J.; Cai, B.; Yang, X.; Sun, L. Efficient and Stable Inverted Planar Perovskite Solar Cells Employing CuI as Hole-Transporting Layer Prepared by Solid–Gas Transformation. *Energy Technology* **2017,** *5* (10), 1836-1843, DOI: 10.1002/ente.201700422.
(20) Ye, S.; Rao, H.; Zhao, Z.; Zhang, L.; Bao, H.; Sun, W.; Li, Y.; Gu, F.; Wang, J.; Liu, Z.; Bian, Z.; Huang, C. A Breakthrough Efficiency of 19.9% Obtained in Inverted Perovskite Solar Cells by Using an Efficient Trap State Passivator Cu(thiourea)I. *Journal of the American Chemical Society* **2017,** *139* (22), 7504-7512, DOI: 10.1021/jacs.7b01439.
(21) Heasley, R.; Davis, L. M.; Chua, D.; Chang, C. M.; Gordon, R. G. Vapor Deposition of Transparent, p-Type Cuprous Iodide Via a Two-Step Conversion Process. *ACS Applied Energy Materials* **2018,** *1* (12), 6953-6963, DOI: 10.1021/acsaem.8b01363.
(22) Balog, Á.; Samu, G. F.; Kamat, P. V.; Janáky, C. Optoelectronic Properties of CuI Photoelectrodes. *The Journal of Physical Chemistry Letters* **2019,** *10* (2), 259-264, DOI: 10.1021/acs.jpclett.8b03242.
(23) Yang, C.; Kneiß, M.; Schein, F.-L.; Lorenz, M.; Grundmann, M. Room-temperature Domain-epitaxy of Copper Iodide Thin Films for Transparent CuI/ZnO Heterojunctions with High Rectification Ratios Larger than 109. *Scientific Reports* **2016,** *6* (1), 21937-21937, DOI: 10.1038/srep21937.
(24) Cha, J.-H.; Jung, D.-Y. Air-Stable Transparent Silver Iodide–Copper Iodide Heterojunction Diode. *ACS Applied Materials & Interfaces* **2017,** *9* (50), 43807-43813, DOI: 10.1021/acsami.7b14378.
(25) Yamada, N.; Kondo, Y.; Cao, X.; Nakano, Y. Visible-blind wide-dynamic-range fast-response self-powered ultraviolet photodetector based on CuI/In-Ga-Zn-O heterojunction. *Applied Materials Today* **2019,** *15*, 153-162, DOI: https://doi.org/10.1016/j.apmt.2019.01.007.
(26) Liu, C.; Peng, M.; Yu, A.; Liu, J.; Song, M.; Zhang, Y.; Zhai, J. Interface engineering on p-CuI/n-ZnO heterojunction for enhancing piezoelectric and piezo-phototronic performance. *Nano Energy* **2016,** *26*, 417-424, DOI: 10.1016/j.nanoen.2016.05.041.
(27) Choi, C.-H.; Gorecki, J. Y.; Fang, Z.; Allen, M.; Li, S.; Lin, L.-Y.; Cheng, C.-C.; Chang, C.-H.; Lin, H.; Yu, J. S.; Chang, R. P. H.; Bedzyk, M. J.; Ferragut, R.; Marks, T. J.; Facchetti, A. Low-temperature, inkjet printed p-type copper(i) iodide thin film transistors. *J. Mater. Chem. C* **2016,** *4* (43), 10309-10314, DOI: 10.1039/C6TC03234F.
(28) Luo, W.; Zeng, C.; Du, X.; Leng, C.; Yao, W.; Shi, H.; Wei, X.; Du, C.; Lu, S. Copper thiocyanate/copper iodide based hole transport composites with balanced properties for efficient polymer light-emitting diodes. *Journal of Materials Chemistry C* **2018**, DOI: 10.1039/C7TC04842D.
(29) Ahn, D.; Park, S.-H. Cuprous halides semiconductors as a new means for highly efficient light-emitting diodes. *Scientific Reports* **2016,** *6* (1), 20718-20718, DOI: 10.1038/srep20718.
(30) Mulla, R.; Rabinal, M. K. Defect-Controlled Copper Iodide: A Promising and Ecofriendly Thermoelectric Material. *Energy Technology* **2017,** *6* (6), 1178-1185, DOI: 10.1002/ente.201700708.
(31) Morais Faustino, B. M.; Gomes, D.; Faria, J.; Juntunen, T.; Gaspar, G.; Bianchi, C.; Almeida, A.; Marques, A.; Tittonen, I.; Ferreira, I. CuI p-type thin films for highly transparent thermoelectric p-n modules. *Scientific Reports* **2018,** *8* (1), 6867, DOI: 10.1038/s41598-018-25106-3.
(32) Herrick, C. S. Oxygen-inhibited Grain Growth in Thin Films of Semiconducting Cuprous Iodide. *Nature* **1966,** *211* (5052), 958-959, DOI: 10.1038/211958a0.
(33) Amalina, M. N.; Rusop, M. Investigation on the I2:CuI thin films and its stability over time. *Microelectronic Engineering* **2013,** *108*, 106-111, DOI: 10.1016/J.MEE.2013.02.079.

(34) Zainun, A. R.; Mamat, M. H.; Noor, U. M.; Rusop, M. Particles Size and Conductivity Study of P-Type Copper (I) Iodide (CuI) Thin Film for Solid State Dye-Sensitized Solar Cells. *IOP Conference Series: Materials Science and Engineering* **2011,** *17* (1), 012009-012009, DOI: 10.1088/1757-899X/17/1/012009.
(35) Gammons, C. H.; Yu, Y. The stability of aqueous silver bromide and iodide complexes at 25–300°C: Experiments, theory and geologic applications. *Chemical Geology* **1997,** *137* (3-4), 155-173, DOI: 10.1016/S0009-2541(96)00160-X.
(36) Herrick, C. S.; Tevebaugh, A. D. Oxygen-Controlled Conduction in Thin Films of Cuprous Iodide: A Mixed Valency Anion Semiconductor. *Journal of The Electrochemical Society* **1963,** *110* (2), 119-121, DOI: 10.1149/1.2425687.
(37) Liang, C. C. Conduction Characteristics of the Lithium Iodide-Aluminum Oxide Solid Electrolytes. *Journal of The Electrochemical Society* **1973,** *120* (10), 1289-1289, DOI: 10.1149/1.2403248.
(38) Maier, J. Defect Chemistry and Conductivity Effects in Heterogeneous Solid Electrolytes. *Journal of The Electrochemical Society* **1987,** *134* (6), 1524-1524, DOI: 10.1149/1.2100703.
(39) Sata, N.; Eberman, K.; Eberl, K.; Maier, J. Mesoscopic fast ion conduction in nanometre-scale planar heterostructures. *Nature* **2000,** *408* (6815), 946-949, DOI: 10.1038/35050047.
(40) Zhang, Q.; Pan, J.; Lu, P.; Liu, Z.; Verbrugge, M. W.; Sheldon, B. W.; Cheng, Y. T.; Qi, Y.; Xiao, X. Synergetic Effects of Inorganic Components in Solid Electrolyte Interphase on High Cycle Efficiency of Lithium Ion Batteries. *Nano Letters* **2016,** *16* (3), 2011-2016, DOI: 10.1021/acs.nanolett.5b05283.
(41) Agrawal, R. C.; Gupta, R. K. Superionic solid: composite electrolyte phase – an overview. *Journal of Materials Science* **1999,** *34* (6), 1131-1162, DOI: 10.1023/A:1004598902146.
(42) Bunde, A.; Dieterich, W. *Percolation in Composites*; Kluwer Academic Publishers: 2000.
(43) Sultana, S.; Rafiuddin. Synthesis, characterization and electrical properties of CdI2 doped Al2O3 and TiO2 superionic conductors. *Journal of Alloys and Compounds* **2011,** *509* (41), 9842-9848, DOI: 10.1016/J.JALLCOM.2011.06.102.
(44) Iqbal, M. Z.; Rafiuddin. Enhanced ionic conduction of CdI2Ag2CrO4 and Al2O3 composite solid electrolytes. *Current Applied Physics* **2016,** *16* (9), 974-979, DOI: 10.1016/J.CAP.2016.05.021.
(45) Sultana, S.; Rafiuddin. Behaviour of electrical conductivity in CsI–Al2O3 and CsI–TiO2 systems. *Arabian Journal of Chemistry* **2016,** *9*, S170-S176, DOI: 10.1016/J.ARABJC.2011.02.025.
(46) Wise, H.; Wood, B. J. Defect structure of cuprous iodide and its catalytic properties. *The Journal of Physical Chemistry* **1967,** *71* (13), 4517-4522, DOI: 10.1021/j100872a058.
(47) Fukumoto, T.; Tabuchi, K.; Nakashima, S.; Mituishi, A. Temperature dependence of Raman linewidth and shift in CuI. *Optics Communications* **1974,** *10* (1), 78-80, DOI: 10.1016/0030-4018(74)90109-6.
(48) Rohrer, G. S. "Introduction to Grains, Phases, and Interfaces—an Interpretation of Microstructure," Trans. AIME, 1948, vol. 175, pp. 15–51, by C.S. Smith. *Metallurgical and Materials Transactions A* **2010,** *41* (5), 1063-1100, DOI: 10.1007/s11661-010-0215-5.
(49) Mallick, A. Effect of second phase mobile particles on polycrystalline grain growth: A phase-field approach. *Computational Materials Science* **2013,** *67*, 27-34, DOI: https://doi.org/10.1016/j.commatsci.2012.08.022.

(50) Chang, K.; Kwon, J.; Rhee, C.-K. Role of second-phase particle morphology on 3D grain growth: A phase-field approach. *Computational Materials Science* **2016,** *124*, 438-443, DOI: https://doi.org/10.1016/j.commatsci.2016.08.019.
(51) Chang, K.; Feng, W.; Chen, L.-Q. Effect of second-phase particle morphology on grain growth kinetics. *Acta Materialia* **2009,** *57* (17), 5229-5236, DOI: https://doi.org/10.1016/j.actamat.2009.07.025.
(52) Smith, C. S. Grains, phases, and interfaces:An introduction of microstructure. *Trans.Metall.Soc.AIME* **1948,** *175*, 15-51.
(53) Zener, C. Grains, Phases and Interfaces: An Interpretation of Microstructure. *Trans. AIME* **1948,** *175*, 15-51.
(54) Olgaard, D. L.; Evans, B. Effect of Second-Phase Particles on Grain Growth in Calcite. *Journal of the American Ceramic Society* **1986,** *69* (11), C-272-C-277, DOI: 10.1111/j.1151-2916.1986.tb07374.x.
(55) Wagner, C. The electrical conductivity of semi-conductors involving inclusions of another phase. *Journal of Physics and Chemistry of Solids* **1972,** *33* (5), 1051-1059, DOI: 10.1016/S0022-3697(72)80265-8.
(56) Phipps, J. B.; Whitmore, D. H. Ion transport in LiISiO2 composites. *Solid State Ionics* **1983,** *9-10*, 123-130, DOI: https://doi.org/10.1016/0167-2738(83)90220-5.
(57) Maier, J. HETEROGENEOUS SOLID ELECTROLYTES. In *Superionic Solids and Solid Electrolytes Recent Trends*; Laskar, A. L.; Chandra, S., Eds.; Academic Press: 1989; pp 137-184.
(58) Maier, J. On the heterogeneous doping of ionic conductors. *Solid State Ionics* **1986,** *18-19*, 1141-1145, DOI: https://doi.org/10.1016/0167-2738(86)90323-1.
(59) Maier, J. Defect Chemistry: Composition, Transport, and Reactions in the Solid State; Part I: Thermodynamics. *Angewandte Chemie International Edition in English* **1993,** *32* (3), 313-335, DOI: 10.1002/anie.199303133.
(60) Maier, J. Ionic conduction in space charge regions. *Progress in Solid State Chemistry* **1995,** *23* (3), 171-263, DOI: https://doi.org/10.1016/0079-6786(95)00004-E.
(61) Pötschke, J.; Gestrich, T.; Richter, V. Grain growth inhibition of hardmetals during initial heat-up. *International Journal of Refractory Metals and Hard Materials* **2018,** *72*, 117-125, DOI: https://doi.org/10.1016/j.ijrmhm.2017.12.016.
(62) Pötschke, J.; Richter, V.; Gestrich, T.; Säuberlich, T.; Meese-Marktscheffel, J. A. Grain growth inhibition in ultrafine hardmetals. *International Journal of Refractory Metals and Hard Materials* **2017,** *66*, 95-104, DOI: https://doi.org/10.1016/j.ijrmhm.2017.03.001.
(63) Peres, V.; Bourgeois, L.; Dehaudt, P. Grain growth and Ostwald ripening in chromia-doped uranium dioxide. *Journal de Physique IV Colloque* **1993,** *03* (C7), C7-1477-C7-1480, DOI: 10.1051/jp4:19937231.
(64) Boyer, M.; Alahraché, S.; Genevois, C.; Licheron, M.; Lefevre, F.-X.; Castro, C.; Bonnefont, G.; Patton, G.; Moretti, F.; Dujardin, C.; Matzen, G.; Allix, M. Enhanced Transparency through Second Phase Crystallization in BaAl4O7 Scintillating Ceramics. *Crystal Growth & Design* **2016,** *16* (1), 386-395, DOI: 10.1021/acs.cgd.5b01374.
(65) Sirimanne, P. M.; Soga, T.; Jimbo, T. Identification of various luminescence centers in CuI films by cathodoluminescence technique. *Journal of Luminescence* **2003,** *105* (2-4), 105-109, DOI: 10.1016/S0022-2313(03)00114-5.
(66) Zhou, Y.; lü, M.; Zhou, G.; Wang, S.; Wang, S. Preparation and photoluminescence of γ-CuI nanoparticles. *Materials Letters* **2006,** *60* (17-18), 2184-2186, DOI: 10.1016/J.MATLET.2005.12.093.

(67) Xia, M.; Gu, M.; Liu, X.; Liu, B.; Huang, S.; Ni, C. Luminescence characteristics of CuI film by iodine annealing. *Journal of Materials Science: Materials in Electronics* **2015,** *26* (7), 5092-5096, DOI: 10.1007/s10854-015-3035-y.
(68) Gao, P.; Gu, M.; Liu, X.-L.; Liu, B.; Huang, S.-M. X-ray excited luminescence of cuprous iodide single crystals: On the nature of red luminescence. *Applied Physics Letters* **2009,** *95* (22), 221904-221904, DOI: 10.1063/1.3271174.
(69) Lin, G.; Zhao, F.; Zhao, Y.; Zhang, D.; Yang, L.; Xue, X.; Wang, X.; Qu, C.; Li, Q.; Zhang, L. Luminescence Properties and Mechanisms of CuI Thin Films Fabricated by Vapor Iodization of Copper Films. *Materials* **2016,** *9* (12), DOI: 10.3390/ma9120990.
(70) Gao, P.; Gu, M.; Liu, X.; Zheng, Y.-Q.; Shi, E.-W. Photoluminescence study of annealing effects on CuI crystals grown by evaporation method. *Crystal Research and Technology* **2012,** *47* (7), 707-712, DOI: 10.1002/crat.201100621.
(71) Zi, M.; Li, J.; Zhang, Z.; Wang, X.; Han, J.; Yang, X.; Qiu, Z.; Gong, H.; Ji, Z.; Cao, B. Effect of deposition temperature on transparent conductive properties of γ-CuI film prepared by vacuum thermal evaporation. *physica status solidi (a)* **2015,** *212* (7), 1466-1470, DOI: 10.1002/pssa.201532015.